HOKKAIDO UNIVERSITY

Title	Thymidine phosphorylase imaging probe for differential diagnosis of metabolic dysfunction-associated steatohepatitis
Author(s)	Higashikawa, Kei; Uehara, Riho; Horiguchi, Sawako et al.
Citation	Molecular imaging and biology, 26(6), 1036-1045 https://doi.org/10.1007/s11307-024-01964-4
Issue Date	2024-11-13
Doc URL	https://hdl.handle.net/2115/97310
Rights	This version of the article has been accepted for publication, after peer review (when applicable) and is subject to Springer Nature's AM terms of use, but is not the Version of Record and does not reflect post-acceptance improvements, or any corrections. The Version of Record is available online at: https://doi.org/10.1007/s11307-024-01964-4
Type	journal article
File Information	TP imaging for differential diagnosis of MASH.pdf

Hokkaido University Collection of Scholarly and Academic Papers : HUSCAP

Thymidine phosphorylase imaging probe for differential diagnosis of metabolic dysfunction-associated steatohepatitis

Kei Higashikawa[1], Riho Uehara[2], Sawako Horiguchi[2], Yuki Shibata[1,3,4], Naoto Okubo[2], Yuki Mizuno[1,5], Hironobu Yasui[1,4], Shunsuke Ohnishi[2], Hiroshi Takeda[2], Yuji Kuge[1,5]

[1]Central Institute of Isotope Science, Hokkaido University, Sapporo 060-0815, Japan

[2]Faculty of Pharmaceutical Sciences, Hokkaido University, Sapporo 060-0812, Japan

[3]Graduate School of Biomedical Science and Engineering, Hokkaido University, Sapporo 060-0815, Japan

[4]Faculty of Veterinary Medicine, Hokkaido University, Sapporo 060-0818, Japan

[5]Global Center for Biomedical Science and Engineering, Faculty of Medicine, Hokkaido University, Sapporo 060-0815, Japan

***Corresponding Author:**

Yuji Kuge, Ph.D.

Central Institute of Isotope Science, Hokkaido University

Kita 15, Nishi 7, Kita-ku, Sapporo 060-0815, Japan

Tel.: +81-11-706-6087

Fax: +81-11-706-7862

E-mail: kuge@ric.hokudai.ac.jp

Running title: TYMP imaging probe for MASH

Category: Original article

Abstract

Purpose

Metabolic dysfunction-associated steatotic liver disease (MASLD) comprises simple steatosis (SS), which has a low risk of mortality, and metabolic dysfunction-associated steatohepatitis (MASH), which can progress to liver cirrhosis and hepatocellular carcinoma. Because differentiation between MASH and SS is the most important issue in the diagnosis of MASLD, the establishment of noninvasive diagnostic methods is urgently needed. In this study, we evaluated the potential of [^{123}I]IIMU, a thymidine phosphorylase (TYMP) targeted SPECT imaging probe, for differential diagnosis of MASLD in a preclinical animal model.

Procedures

SS and MASH mice were prepared by feeding db/db mice with a standard diet and a methionine/choline-deficient diet, respectively. Control mice were prepared by feeding m/m mice with a standard diet. TYMP expression in the liver was evaluated by RT-PCR, western blotting, and immunohistochemistry. The biodistribution of [^{125}I]IIMU in the three model mice was evaluated at 30 min post-injection. SPECT/CT imaging studies of the three model mice were performed 30 min after injection of [^{123}I]IIMU.

Results

Hepatic TYMP expression level was the highest in the SS mice and the lowest in the MASH mice at both mRNA and protein levels. The immunohistochemistry experiment showed a patchy distribution of TYMP only in the liver of MASH mice. In the biodistribution study, the hepatic accumulation of [^{125}I]IIMU was the highest in the SS mice and the lowest in the MASH mice. The SPECT/CT imaging study showed similar results to the biodistribution experiment.

Conclusion

Hepatic TYMP expression level may serve as a promising imaging biomarker for differential diagnosis of SS and MASH. SPECT imaging using [^{123}I]IIMU potentially provides a novel noninvasive diagnostic method to differentiate MASH and SS.

KEYWORDS: metabolic dysfunction-associated steatohepatitis (MASH), non-alcoholic steatohepatitis (SS), Thymidine phosphorylase (TYMP), 5-iodo-6-[(2-iminoimidazolidinyl)methyl]uracil (IIMU), Nuclear medicine imaging

Introduction

Metabolic dysfunction-associated steatotic liver disease (MASLD) is a very common disorder that happens when excess fat is accumulated in the liver. MASLD encompasses simple steatosis (SS) which has a low risk of liver disease-related mortality, and non-alcoholic steatohepatitis (MASH) which may progress to liver cirrhosis and hepatocellular carcinoma (HCC). Accordingly, differentiation between MASH and SS is the most important issue in the diagnosis of MASLD. Nowadays, liver biopsy is essential to the differential diagnosis of MASH from SS [1]. However, liver biopsy has several drawbacks, including sampling error (diagnostic results tend to be different depending on the biopsy site), interobserver variability, and procedure-related morbidity and mortality [1-4]. Because of these drawbacks, the establishment of less or noninvasive diagnostic methods to replace biopsy is urgently desired.

Nuclear medicine imaging technologies, single-photon emission tomography (SPECT) and positron emission tomography (PET), can visualize an interest molecule and evaluate disease state in whole organs noninvasively. Therefore, these imaging technologies have a potential to provide the differential diagnosis of MASH, if imaging biomarkers with different expression levels between SS and MASH are found.

To date, several nuclear medicine probes have been investigated for the diagnosis and staging of MASLD [5-6]. For example, [^{18}F]FDG has potential to determine liver inflammation, particularly dynamic PET can derive altered glucose transport (K1) in MASH [7-8]. [^{18}F]FEDAC may be used to image inflammation/fibrosis progression based on its binding to translocator protein (18 kDa) (TSPO) [9-10]. Recently, Song et al. indicated the potential of [^{68}Ga]DOTA-FAPI-04 to visualize liver fibrosis through imaging of fibroblast activation protein (FAP) [11]. However, the clinical application of these probes still remains limited.

We previously found the hepatic expression level of thymidine phosphorylase (TYMP) was significantly lower in the methionine and choline deficient (MCD) diet-induced MASH mice compared with that in the control mice [12]. The underlying cause is unclear. However, a recent study [13] suggested that dysfunction of Hedgehog, a lipid-regulated morphogenic signaling pathway, and decreased TYMP create a vicious cycle that impairs mitochondrial activity and accelerates senescence, thereby leading to MASH. They also suggested that TYMP directly acts on hepatocytes to inhibit lipotoxicity and senescence, protecting against MASH formation. Therefore, TYMP imaging may offer an alternative approach for diagnosing and staging MASLD, by evaluating mitochondrial dysfunction and lipotoxicity associated with dysfunction of

Hedgehog signaling pathway. On the other hand, we have developed TYMP-targeting probe [$^{123/125}$I]5-iodo-6-[(2-iminoimidazolidinyl)methyl]uracil ([$^{123/125}$I]IIMU) [14] and demonstrated that [$^{123/125}$I]IIMU accumulated in cells and tissues, depending on TYMP expression level [15-18], and was safely injected in humans [19]. Furthermore, we found that the hepatic accumulation level of [$^{123/125}$I]IIMU was significantly lower in the MASH mice compared with that in the control mice, being consistent with the expression levels of TYMP [12]. However, there have been no studies to investigate whether the hepatic expression of TYMP is different between SS and MASH, and whether TYMP imaging is applicable to the differential diagnosis of MASH. Therefore, in this study, we compared the hepatic TYMP expression levels among SS and MASH models and control mice, and evaluated the potentials of a TYMP-targeting probe [^{123}I]IIMU for the differential diagnosis of MASH from SS.

Materials and Methods

Preparation of mouse SS and MASH models

Male obese mice (db/db mice; BKS. Cg-+Lepr^{db}/+Lepr^{db}/Jcl), and gender and age matched lean mice (m/m mice; BKS. Cg-m+/m+/Jcl) were purchased from CLEA Japan, Inc. (Tokyo, Japan). These mice were housed under a 12-h light/12-h dark cycle with food and water supplied ad libitum. All experimental protocols were approved by the Laboratory Animal Care and Use Committee of Hokkaido University and performed in accordance with the Guidelines for Animal Experiments of the Graduate School of Medicine, Hokkaido University.

SS and MASH mice were prepared by feeding the db/db mice (8 weeks old) with a standard diet (CE-2, CLEA Japan, Inc.) and a methionine/choline-deficient (MCD) diet (A02082002B, Research Diet, Inc.) for 4 weeks, respectively. Control mice were prepared by feeding the m/m mice (8 weeks old) with the standard diet for 4 weeks.

Real-time reverse-transcription polymerase chain reaction (RT-PCR) analysis

RNA extraction and purification, reverse transcription of mRNA, and PCR analysis were performed in the same way as our previous studies [12]. Total RNA was isolated from the liver of control, SS, and MASH mice with TRIZOL® reagent (Thermo Fisher Scientific Inc., Waltham, MA) and purified with a PureLink™ RNA Mini Kit (Thermo Fisher Scientific Inc.). Reverse transcription of the total RNA (500 ng) was then performed using a ReverTra Ace® qPCR RT Master Mix with a gDNA Remover (TOYOBO Co., Ltd., Osaka, Japan) and a PCR Thermal Cycler Dice (Takara Bio Inc., Kusatsu, Japan). The gene expression levels of TNF-α, interleukin-1β (IL-1β), collagen type I alpha 1 (COL1A1), collagen type I alpha 2 (COL1A2), α-smooth muscle actin (α-SMA), and TATA-binding protein (TBP) were analyzed by real-time RT-PCR using FastStart Universal SYBR Green Master (Rox) (Roche Diagnostics, Indianapolis, IN), the primer set specific for each molecule, and Thermal Cycler Dice Real Time System II. Primer sequences are listed in Supplementary Table S1. The expression level of TYMP was examined by real-time RT-PCR analysis using primer-probe sets of TaqMan Gene Expression Assays (Mm00460357_m1; Thermo Fisher Scientific Inc.), TaqMan™ Universal Master Mix II, with UNG (Thermo Fisher Scientific Inc), and Thermal Cycler Dice Real Time System II (Takara Bio Inc.). TBP was used as an internal control, and each gene expression level was normalized with that of TBP.

Western blot analysis

The liver samples of control, SS, and MASH mice were homogenized in RIPA Lysis and Extraction Buffer (Thermo Fisher Scientific, Inc.) containing a protease inhibitor cocktail (cOmplete™, Roche Co., Ltd., Mannheim, Germany) and then centrifuged to remove insoluble products. The proteins (1-20 μg), recombinant uridine phosphorylase 1 (rUPP1; 1 ng; Cloud-Clone Co., Katy, TX), and rUPP2 (10 ng ; Cloud-Clone Co.) were separated by sodium dodecyl sulfate polyacrylamide gel electrophoresis (SDS-PAGE) on a 5–20% polyacrylamide. Proteins were transferred onto polyvinylidene fluoride membranes (Bio-Rad Laboratories, Inc. Hercules, CA). The membranes were washed with 25 mM Tris–HCl, 137 mM NaCl, and 2.68 mM KCl (pH 7.4) (TBS buffer), and then blocked with 50 mM Tris–HCl, 138 mM NaCl, 2.70 mM KCl, and 0.5 ml/L Tween 20 (pH 8.0) (TBS-T buffer) plus 5% skim milk. The membranes were incubated with a sheep polyclonal anti-TYMP primary antibody (1:1000; R&D Systems, Inc., Minneapolis, MN) or a rabbit monoclonal anti-TBP primary antibody (1:1000; Cell Signaling Technology Inc., Beverly, MA), an anti-UPP1 primary antibody (1:400; Lifespan Biosciences Inc., Seattle, WA), and an

anti-UPP2 primary antibody (1:3000; Abcam, Inc., Cambridge, UK) diluted in TBS-T buffer plus 5% skim milk. The membranes were washed with TBS-T buffer and incubated with a horseradish peroxidase (HRP)-conjugated anti-sheep secondary antibody (1:1000; R&D Systems, Inc.) or anti-rabbit secondary antibody (1:4000; Promega Inc., Madison, WI) diluted in TBS-T buffer plus 5% skim milk. The proteins of interest were detected using the ECL Prime Western Blotting Detection Reagent (GE Healthcare Inc., Chicago, IL) and the luminescent image analyzer LAS-4000 mini (Fuji Photo Film Co., Ltd., Tokyo, Japan). TBP was used as the protein-loading control for immunoblotting.

Histopathological evaluation

Hematoxylin and eosin (H&E)-staining was performed in the same way as our previous studies [12] using 5-μm-thick liver sections embedded in paraffin.

Masson's trichrome staining was performed as follows. Five-micrometer-thick liver sections embedded in paraffin were heated in Bouin’s Solution (HT10132; Merck KGaA, Darmstadt, Germany) at 56°C for 15 minutes and washed in running water. The sections were stained with Weigert’s iron hematoxylin solution (HT1079; Merck

KGaA), washed in running water, and rinsed in deionized water. The sections were stained in Biebrich Scarlet-Acid Fucshin Solution (HT151; Merck KGaA) for 5 minutes, washed in running water, and rinsed in deionized water. The sections were placed in Phosphotungstic/Phosphomolybdic Acid Solution (HT152-153; Merck KGaA) for 5 minutes, washed in running water, and rinsed in deionized water. Then, the sections were stained with Aniline Blue Solution (HT154; Merck KGaA) for 5 minutes. The sections were placed in 1% acetic acid for 2 minutes and washed in deionized water. Finally, the sections were dehydrated in an ethanol series, placed in xylene, and mounted.

Immunohistochemical (IHC) staining of TYMP was performed as follows. The livers were embedded in Optimal Cutting Temperature (O.C.T.) compound (Sakura Finetek Japan Co., Ltd., Tokyo, Japan) and frozen in isopentane/dry ice. Ten-μm-thick frozen tissue sections were prepared and mounted on MAS-coated glass slides (Matsunami Glass Ind., Co., Ltd., Kishiwada, Japan) and fixed with M-Fix™ spray fixative (Merck KGaA). The hepatic tissue sections were washed in 100 mL of phosphate-buffered saline (-) [PBS (-)] containing a drop of 13-fold diluted Triton-X, and blocked with a blocking solution (protein block, serum-free; Agilent Technologies, Inc., Carpinteria, CA). The tissue sections were incubated with an anti-TYMP antibody (1:100; R&D

Systems, Inc.) in 0.1% BSA/PBS (-) and washed in the PBS (-) plus the Triton-X solution. Endogenous peroxidase inactivation of the tissue section was performed with 0.3% H_2O_2/methanol. The tissue sections were washed in the PBS (-) plus the Triton-X solution, incubated with an HRP-conjugated anti-sheep antibody (1:100; R&D Systems, Inc.) in 0.1% BSA/PBS (-), and washed with PBS (-). Immunocomplexes were detected with a Peroxidase Stain DAB Kit (Nacalai Tesque Inc., Kyoto, Japan) and counterstained with hematoxylin.

Biodistribution study

[^{125}I]IIMU (44-99 kBq) [14] in saline was injected to the control, SS, and MASH mice via the tail vein under isoflurane anesthesia. Then, the mice were returned to their cages and allowed to move freely. Thirty minutes after the injection, the mice were euthanized under isoflurane anesthesia, and their blood and organs were immediately collected. After washing the organs with saline, the blood and the organs were weighed. The radioactivity in the blood and organs was measured with a gamma counter (2480 WIZARD 2 Automatic Gamma Counter, PerkinElmer Inc., Waltham, MA). Decay-corrected accumulation in the blood and organs was expressed as standardized

uptake value (SUV). SUV was defined as [tissue radioactivity concentration (Bq/g)/injected radioactivity (Bq)] × body weight (g).

Small animal SPECT/CT imaging study

A SPECT/CT imaging study was performed on control, SS, and MASH model mice (n = 4 for each) using an Inveon preclinical small-animal multimodality SPECT/CT system (Siemens Medical Solutions, Knoxville, TN, USA) equipped with a single pinhole collimator (1-MHS-2.0). Mice were intravenously injected with [^{123}I]IIMU (4.6-8.3 MBq) in saline containing 1% ascorbic acid via tail vein under isoflurane anesthesia. SPECT data were acquired over 30-45 min after the injection, and CT scans were performed after SPECT acquisitions. The SPECT and CT images were reconstructed using OSEM3D (8 iterations, 6 subsets) and the Feldkamp method, respectively. The isotropic image voxel sizes of the SPECT and CT images were 0.5 mm and 92.7 μm, respectively. For SPECT image reconstruction, attenuation correction was performed based on the CT images, and scatter correction was applied using the triple energy window method. The obtained images were analyzed using an Inveon research workplace software (Siemens Medical Solutions, Knoxville, TN, USA). All

SPECT/CT fusion images (coronal slices) are displayed on the same SUV scale ranging from 0 to 7.

Statistical analysis

All data are expressed as means ± standard deviation (SD) and analyzed using one-way analysis of variance (ANOVA) followed by Tukey-Kramer test. The level of significance was taken as $p < 0.05$. All statistical analysis was carried out using GraphPad Prism 7 software (GraphPad Software Inc., San Diego, CA).

Results

Physiological characteristic and pathological evaluation in control, SS, and MASH mice

Body and liver weights in the control, SS, and MASH mice are shown in Fig. 1. The SS and MASH mice had higher body weight than the control mice whereas the MASH mice had lower body weight than the SS mice [Body weight: 22.3 ± 0.7 (Control), 40.2 ± 2.2 (SS), 32.7 ± 0.4 (MASH)] (Fig. 1a). On the other hand, the liver weight was the highest in the MASH mice, followed in the decreasing order by the SS and control mice [Liver: 0.923 ± 0.016 (Control), 1.510 ± 0.333 (SS), 2.210 ± 0.222 (MASH)] (Fig. 1b).

The hepatic gene expression levels of inflammation (TNF-α, IL-1β) and fibrosis markers (COL1A1, COL1A2, α-SMA) in the control, SS, and MASH mice are shown in Fig. 2. The expression levels of TNF-α, IL-1β, COL1A1, COL1A2, and α-SMA were significantly higher in the MASH mice than in the control and SS mice, whereas there were no significant changes in the markers between the control and SS mice. Figure 3 displays H&E and Masson's trichrome-stained liver sections from the control, SS, and MASH mice. Prominent steatosis, cellular infiltration, and ballooning degeneration of

hepatocytes were observed in the MASH model mice, whereas only steatosis was observed in the SS model mice (Fig. 3, panel a-c). The above histological features were not observed in the liver of control mice. Hepatic fibrosis was observed in 2 out of 5 MASH mice, whereas not in the control and SS mice (Fig. 3, panel d-f).

Hepatic TYMP and UPP expressions in control, SS, and MASH mice

The hepatic gene expression levels of TYMP were significantly higher in SS mice and tended to be lower in MASH mice than in the control mice [relative expression of mRNA: 1.00 ± 0.32 (Control), 1.72 ± 0.27 (SS), 0.58 ± 0.13 (MASH)] (Fig. 4a). Similarly, the TYMP protein levels was higher in the SS mice and lower in the MASH mice (Fig. 4b). UPP1 and UPP2 were not detected in all mice, whereas rUPP1 (1 ng) and rUPP2 (10 ng) (positive controls) were clearly detected (Fig. S1).

Hepatic localizations of TYMP protein in control, SS, and MASH mice

Representative IHC staining of TYMP are shown in Fig. 4, panel c-e. TYMP was entirely distributed in the liver of the control and SS mice, whereas it showed a patchy distribution in the liver of the MASH mice.

Biodistribution analyses of [^{125}I]IIMU in control, SS, and MASH mice

The biodistribution of [^{125}I]IIMU in the control, SS, and MASH mice, 30 min after administration are shown in Fig. 5. [^{125}I]IIMU highly accumulated in the liver and small intestine compared to other organs including the heart, lung, pancreas, spleen, stomach, large intestine, kidney, and thigh muscle and bone. The hepatic accumulation level of [^{125}I]IIMU was significantly higher in the SS mice and lower in the MASH mice than the control mice [standard uptake value (SUV) : 5.40 ± 1.29 (Control), 7.25 ± 0.58 (SS), 3.39 ± 0.39 (MASH)]. Furthermore, the hepatic accumulation level of [^{125}I]IIMU was significantly lower in MASH mice than the SS mice ($p < 0.001$). The accumulation level in the small intestine of the SS and MASH mice was significantly higher than that of the control mice, whereas there were no significant differences between the SS and MASH mice [standard uptake value (SUV): 1.23 ± 0.21 (Control), 2.39 ± 0.81 (SS), 2.91 ± 0.21 (MASH)].

SPECT/CT imaging of [^{123}I]IIMU in control, SS, and MASH mice

Representative SPECT/CT images of the control, SS, and MASH mice after the injection of [^{123}I]IIMU are shown in Fig. 6 and Fig. S2. The liver uptake of [^{123}I]IIMU in MASH mice was visually lower than that in SS and control mice.

Discussion

To the best of our knowledge, this is the first study to compare the hepatic expression levels of TYMP among the control, SS, and MASH mice and to examine the usability of a TYMP imaging probe for differentiating MASH from SS. We found that the hepatic expression levels of TYMP were higher in the SS mice and lower in the MASH mice than in the control mice (Fig. 4, panel a-b). TYMP was distributed in a patchy fashion in the liver of MASH mice, whereas it was evenly distributed in the liver of control and SS mice (Fig. 4, panel c-e). Consistent with these different expression levels of TYMP in the liver, the hepatic accumulation of [^{125}I]IIMU were significantly lower in the MASH mice than in the control and SS mice (Fig. 5). Finally, SPECT imaging using [^{123}I]IIMU provided visually distinguishable images between SS and MASH model mice, suggesting the usefulness of [^{123}I]IIMU-SPECT as a non-invasive means for the differential diagnosis of MASH.

We previously reported that the gene and protein of TYMP were more highly expressed in the normal liver and small intestine than in the other normal organs, including the brain, heart, lung, stomach, spleen, kidney, large intestine, and muscle [16]. [$^{123/125}$I]IIMU also accumulated mostly in the liver and small intestine of normal,

MASH, and tumor bearing mice [12, 14, 16, 18]. Moreover, we performed the blocking study in MCD diet-induced MASH and control mice using tipiracil [12]. The tipiracil is a TYMP inhibitor and has a similar chemical structure to IIMU. In the blocking study, the accumulation of [^{123}I]IIMU in the liver and small intestine of both MASH and control mice was significantly reduced [12]. These results suggested that the accumulation of [^{123}I]IIMU in the liver and small intestine is ascribed to its binding to the TYMP expressed in the liver and small intestine. Together, the present results indicate that [^{123}I]IIMU has a potential of differentiating MASH from SS based on the expression levels of TYMP.

It is crucial, however, to discuss why the TYMP level and [$^{123/125}$I]IIMU accumulation (SUV) in the liver were higher in SS mice and lower in MASH mice compared to controls. As mentioned above, JUN et al. (2024) [13] recently reported that dysfunction of Hedgehog signaling pathway decreases TYMP levels (and vise versa), leading to reduced mitochondrial activity and increased susceptibility to lipotoxicity, thereby causing MASH. These findings likely explain the lower TYMP level and [$^{123/125}$I]IIMU accumulation (SUV) in MASH mice. On the other hand, the reason for the higher TYMP level and [$^{123/125}$I]IIMU accumulation (SUV) in SS mice remains unclear. Based on the findings by Jun et al. (2024) and the role of TYMP in maintaining mitochondrial

integrity and optimizing DNA repair [20], TYMP appears to play a protective role against MASLD progression. Thus, the higher TYMP level and [$^{123/125}$I]IIMU accumulation (SUV) in SS mice may reflect an adaptive response protecting hepatocytes from injury.

Significant differences in body and liver weights were observed among the three groups of mice (Fig. 1). Therefore, their effects on hepatic [$^{123/125}$I]IIMU accumulation must be considered. We used SUV, corrected for body and liver weights, to evaluate hepatic [^{125}I]IIMU accumulation (Fig. 5), which is widely used in clinical settings. However, this correction may overestimate hepatic accumulation of labeled probes in cases of high body and liver fat contents and low probe distribution in fat. Conversely, without correction, hepatic accumulation may be underestimated. Indeed, without body weight correction, the difference in hepatic accumulation of [^{125}I]IIMU between the SS and control mice was eliminated, suggesting the need to consider the influence of body weight including body fat content (Fig. S3). On the other hand, even without body weight correction, hepatic accumulation of [^{125}I]IIMU in MASH mice remained significantly lower than in SS and control mice. Unfortunately, the current data on body and hepatic fat content, as well as the distribution of [$^{123/125}$I]IIMU in fat, are insufficient. This limitation complicates appropriate corrections and requires further

studies. Although extensive research on the correction methods has been conducted for [^{18}F]FDG, these methods have not yet been widely adopted [21-22].

In this study, we utilized the db/db mice fed with the standard and MCD diet as SS and MASH models, respectively. The db/db mice have persistent hyperphagia, and are obese and diabetic, because their leptin receptor function is deficient [23]. Although the db/db mice have hepatic steatosis, they do not spontaneously develop MASH. Moreover, MASH can be easily induced when the db/db mice are given with a methionine and choline-deficient diet. Therefore, db/db mice alone and the mice fed with the MCD-diet are good models of SS and MASH, respectively [23]. Also in our study, although the body weight of MASH mice was lower than that of SS mice due to MCD diet feeding [12, 24], both SS and MASH mice had higher body and liver weights than the control mice (Fig. 1). The hepatic expression levels of markers of inflammation and fibrosis (Fig. 2) were significantly higher in the MASH mice than in the control mice, while there were no significant changes between the control and SS mice. Furthermore, the main histopathological features of MASH, such as prominent steatosis, cellular infiltrations, and ballooning degeneration of hepatocytes, were observed in the liver of MASH mice, whereas only steatosis was observed in the SS model mice (Fig. 3, panel a-c). The hepatic fibrosis was observed only in 2 out of 5 MASH mice and not in the

control and SS mice (Fig. 3, panel d-f). These results indicated that MASH model without fibrosis or with mild fibrosis, and SS model were successfully prepared in our study.

It should be noted that [$^{123/125}$I]IIMU may accumulate organs expressing the UPPs, since mouse UPPs (UPP1 and UPP2) also have TYMP activity unlike human UPPs [25]. Unfortunately, we have not examined whether UPP affects the biodistribution of [^{125}I]IIMU. However, our study clearly revealed that UPP1 and UPP2 expressions were not detected in the liver of the control, SS, and MASH mice (Fig. S1), indicating that UPPs are not involved in the hepatic accumulation of the IIMU.

To date, various noninvasive imaging methods have been established for the diagnosis of MASLD patients, such as ultrasonography (US), computed tomography (CT), magnetic resonance imaging (MRI), and elastographic imaging. Although US, CT, and MRI are highly useful for quantifying hepatic steatosis, it is difficult to distinguish MASH from SS by using these conventional techniques [2]. The elastographic imaging, including magnetic resonance elastography (MRE) and ultrasound elastography (UE), are promising imaging methods to measure liver stiffness (i.e. the degree of liver fibrosis) [2, 26]. The elastographic imaging has the potential to differentiate MASH

with hepatic fibrosis from SS. However, the performance of elastographic imaging to diagnose MASH without significant fibrosis is unknown but appears to be limited. On the other hand, this study demonstrated that the accumulation levels of [^{125}I]IIMU were lower in the liver of MASH mice without fibrosis or with mild fibrosis, when compared to those of the control and SS mice. [^{123}I]IIMU may be applicable to the differential diagnosis of MASH at early stage, although the reason for the different hepatic expression levels of TYMP among the control, SS and MASH mice is to be clarified.

Conclusions

The hepatic expression levels of TYMP were significantly lower in the MASH mice with the patchy distribution, whereas significantly higher in the SS mice, in comparison with the control mice. The hepatic accumulation levels of [^{125}I]IIMU were consistent with the hepatic expression levels of TYMP. These results indicated that the expression level and distribution of TYMP are promising imaging biomarkers of MASH, and SPECT imaging using [^{123}I]IIMU may be applicable to the differential diagnosis of MASH and SS.

Acknowledgments

The authors thank Mr. Makoto Tarisawa, Ms. Haruka Takahashi, and Ms. Haruka Miura for their technical support in the biodistribution of [^{125}I]IIMU. This study was supported in part by Grants-in-Aid for Scientific Research (Grant number: 19K17255) from the Japan Society for the Promotion of Science and the Ministry of Education, Culture, Sports, Science, and Technology, Japan.

Conflict of Interest Statement

Yuji Kuge, Hokkaido University, and Health Sciences University of Hokkaido had patent rights for [^{123}I]IIMU, but the patent rights has been expired. Yuji Kuge has received grants from Nihon Medi-Physics Co.,Ltd., grants from ATOX Co.,Ltd., grants from Sumitomo Heavy Industries, Ltd., grants from Advanced Medical Science-Planning, Inc, personal fees for consultation from Ono Pharmaceutical Co., Ltd., personal fees for consultation from Novartis Pharma K.K., outside the submitted work. Kei Higashikawa is presently an employee of CHUGAI PHARMACEUTICAL CO., LTD. There are no other potential conflicts of interest relevant to this article.

References

1. Sumida Y, Nakajima A, Itoh Y (2014) Limitations of liver biopsy and non-invasive diagnostic tests for the diagnosis of nonalcoholic fatty liver disease/nonalcoholic steatohepatitis. World J Gastroenterol 20:475-485.
2. Li Q, Dhyani M, Grajo JR, Sirlin C, Samir AE (2018) Current status of imaging in nonalcoholic fatty liver disease. World J Gastroenterol 10:530-542.
3. Gawrieh S, Knoedler DM, Saeian K, Wallace JR, Komorowski RA (2011) Effects of interventions on intra- and interobserver agreement on interpretation of nonalcoholic fatty liver disease histology. Ann Diagn Pathol 15:19-24.
4. Younossi ZM, Gramlich T, Liu YC, et al. (1998) Nonalcoholic fatty liver disease: assessment of variability in pathologic interpretations. Modern pathology : an official journal of the United States and Canadian Academy of Pathology, Inc 11:560-565.
5. Shao T, Josephson L, Liang SH (2019) PET/SPECT Molecular Probes for the Diagnosis and Staging of Nonalcoholic Fatty Liver Disease. Molecular imaging 18:1536012119871455.
6. Wegrzyniak O, Rosestedt M, Eriksson O (2021) Recent Progress in the Molecular Imaging of Nonalcoholic Fatty Liver Disease. International Journal of Molecular Sciences 22:7348.
7. Sarkar S, Matsukuma KE, Spencer B, et al. (2021) Dynamic Positron Emission Tomography/Computed Tomography Imaging Correlate of Nonalcoholic Steatohepatitis. Clin Gastroenterol Hepatol 19:2441-2443.
8. Sarkar S, Corwin MT, Olson KA, et al. (2019) Pilot Study to Diagnose Nonalcoholic Steatohepatitis With Dynamic ^{18}F-FDG PET. Am J Roentgenol 212:529-537.
9. Hatori A, Yui J, Xie L, et al. (2015) Utility of Translocator Protein (18 kDa) as a Molecular Imaging Biomarker to Monitor the Progression of Liver Fibrosis. Sci Rep 5:17327.
10. Xie L, Yui J, Hatori A, et al. (2012) Translocator protein (18kDa), a potential molecular imaging biomarker for non-invasively distinguishing non-alcoholic fatty liver disease. J Hepatol 57:1076-1082.
11. Song Y, Qin C, Chen Y, et al. (2024) Non-invasive visualization of liver fibrosis with [^{68}Ga]Ga-DOTA-FAPI-04 PET from preclinical insights to clinical

translation. European Journal of Nuclear Medicine and Molecular Imaging. Online ahead of print, doi: 10.1007/s00259-024-06773-z.
12. Higashikawa K, Horiguchi S, Tarisawa M, et al. (2020) Preclinical investigation of potential use of thymidine phosphorylase-targeting tracer for diagnosis of nonalcoholic steatohepatitis. Nucl Med Biol 82-83:25-32.
13. Jun JH, Du K, Dutta RK, et al. (2024) The senescence-associated secretome of hedgehog-deficient hepatocytes drives MASLD progression. The Journal of Clinical Investigation. e180310.
14. Takahashi M, Seki K, Nishijima K, et al. (2008) Synthesis of a radioiodinated thymidine phosphorylase inhibitor and its preliminary evaluation as a potential SPECT tracer for angiogenic enzyme expression. Journal of Labelled Compounds and Radiopharmaceuticals 51:384-387.
15. Kobashi N, Matsumoto H, Zhao S, et al. (2016) The Thymidine Phosphorylase Imaging Agent ^{123}I-IIMU Predicts the Efficacy of Capecitabine. J Nucl Med 57:1276-1281.
16. Zhao S, Li H, Nishijima K, et al. (2015) Relationship between biodistribution of a novel thymidine phosphorylase (TP) imaging probe and TP expression levels in normal mice. Ann Nucl Med 29:582-587.
17. Li H, Zhao S, Jin Y, et al. (2011) Radiolabeled uracil derivative as a novel SPECT probe for thymidine phosphorylase: suppressed accumulation into tumor cells by target gene knockdown. Nucl Med Commun 32:1211-1215.
18. Akizawa H, Zhao S, Takahashi M, et al. (2010) In vitro and in vivo evaluations of a radioiodinated thymidine phosphorylase inhibitor as a tumor diagnostic agent for angiogenic enzyme imaging. Nucl Med Biol 37:427-432.
19. Watanabe S, Nishijima K, Okamoto S, et al. (2020) Biodistribution and internal radiation dosimetry of a novel probe for thymidine phosphorylase imaging, [^{123}I]IIMU, in healthy volunteers. Ann Nucl Med 34:595-599.
20. Li W, Yue H (2018) Thymidine phosphorylase: A potential new target for treating cardiovascular disease. Trends Cardiovasc Med 28:157-171.
21. Ustsinau U, Kulterer OC, Rausch I, et al. (2024) A PET/MRI study on the effect of obesity and NAFLD on hepatic [^{18}F]FDG uptake. Eur J Radiol 177:111552.
22. Keramida G, Peters AM (2020) FDG PET/CT of the non-malignant liver in an increasingly obese world population. Clinical Physiology and Functional Imaging 40:304-319.
23. Lau JKC, Zhang X, Yu J (2017) Animal models of non-alcoholic fatty liver disease: current perspectives and recent advances. The Journal of Pathology 241:36-44.

24. Stephenson K, Kennedy L, Hargrove L, et al. (2018) Updates on Dietary Models of Nonalcoholic Fatty Liver Disease: Current Studies and Insights. Gene Expression 18:5-17.
25. Haraguchi M, Tsujimoto H, Fukushima M, et al. (2002) Targeted Deletion of Both Thymidine Phosphorylase and Uridine Phosphorylase and Consequent Disorders in Mice. Molecular and Cellular Biology 22:5212-5221.
26. Lee SS, Park SH (2014) Radiologic evaluation of nonalcoholic fatty liver disease. World J Gastroenterol 20:7392-7402.

Figure legends

Fig. 1 Anthropometric measurements of control, SS, and MASH mice. (**a**) Body weights of the control, SS, and MASH mice (n = 4 - 5). (**b**) Liver weights of the control, SS, and MASH mice. Data are expressed as means (bar: standard deviation). For statistical evaluation, one-way ANOVA followed by Tukey-Kramer's test was applied. The symbols ** and *** denote $p < 0.01$ and $p < 0.001$, respectively.

Fig. 2 Hepatic gene expression level in control, SS, and MASH mice by real-time RT-PCR. Relative hepatic expression levels of inflammatory (TNF-α, IL-1β) and fibrosis (COL1A1, COL1A2, α-SMA) markers in the control (n = 5), SS (n = 5), and MASH mice (n = 5). Each expression level was normalized to that of TBP. Data are expressed as means (bar: standard deviation). For statistical evaluation, one-way ANOVA followed by Tukey-Kramer's test was applied. The symbols * and *** denote $p < 0.05$ and $p < 0.001$, respectively.

Fig. 3 Histopathological evaluation in the liver of the control, SS, and MASH mice. Representative H&E-staining in the control (**a**), SS (**b**), and MASH (**c**) mice are shown.

The yellow and blue arrows indicate cellular infiltration and ballooning degeneration of hepatocytes, respectively. Representative Masson's trichrome-staining in the control (**d**), SS (**e**), and MASH (**f**) mice are shown. The green arrow indicates the region of fibrosis. Scale bar = 100 μm.

Fig. 4 TYMP expression in the liver of the control, SS, and MASH mice. (**a**) Hepatic gene expression levels of TYMP were evaluated in the control (n = 5), SS (n = 5), and MASH mice (n = 5) by real-time RT-PCR. Each TYMP expression level was normalized to that of TBP. Data are expressed as means (bar: standard deviation). For statistical evaluation, one-way ANOVA followed by Tukey-Kramer's test was applied. The symbols * and *** denote $p < 0.05$ and $p < 0.001$, respectively. (**b**) Hepatic protein expression of TYMP were evaluated in the control, SS, and MASH mice by western blot analyses. The expression levels of TBP are shown as an internal control. Representative IHC staining of TYMP in the liver of the control (**c**), SS (**d**), and MASH (**e**) mice are shown. Scale bar = 200 μm.

Fig. 5 Biodistribution of [^{125}I]IIMU in the control, SS, and MASH mice. Data show SUVs of [^{125}I]IIMU in the control (n = 4), SS (n = 4), and MASH mice (n = 4) and are

expressed as means (bar: standard deviation). For statistical evaluation, one-way ANOVA followed by Tukey-Kramer's test was applied. The symbol *, **, and *** denote $p < 0.05$, $p < 0.01$, and $p < 0.001$, respectively.

Fig. 6 SPECT/CT images of control, SS, and MASH model mice after injection of [^{123}I]IIMU. All SPECT images (coronal slices) are displayed on the same SUV scale ranging from 0 to 7.

Fig. 1

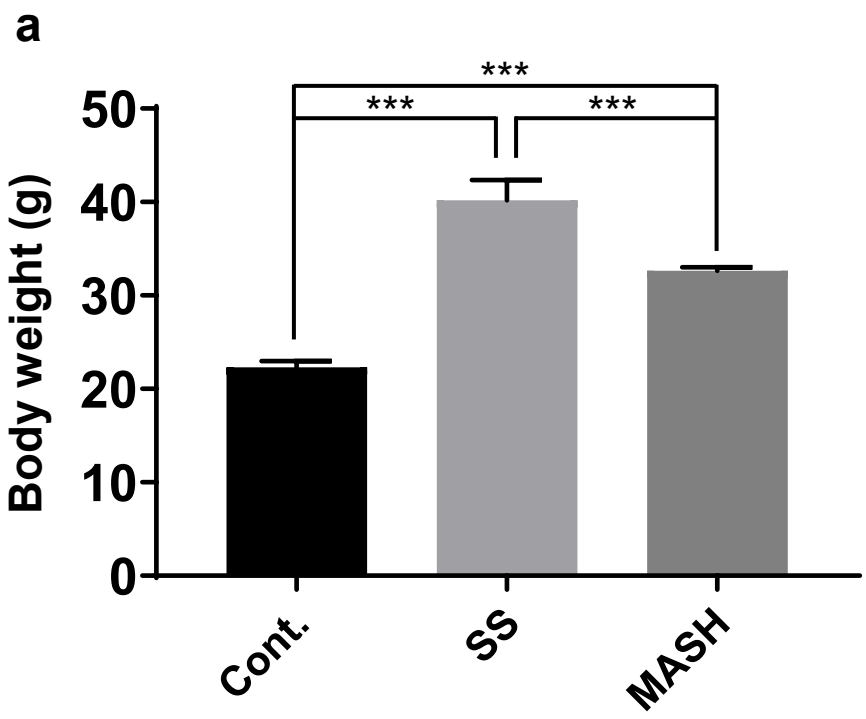
a
Body weight (g)
50
40
30
20
10
0
***
***
***
Cont.
SS
MASH

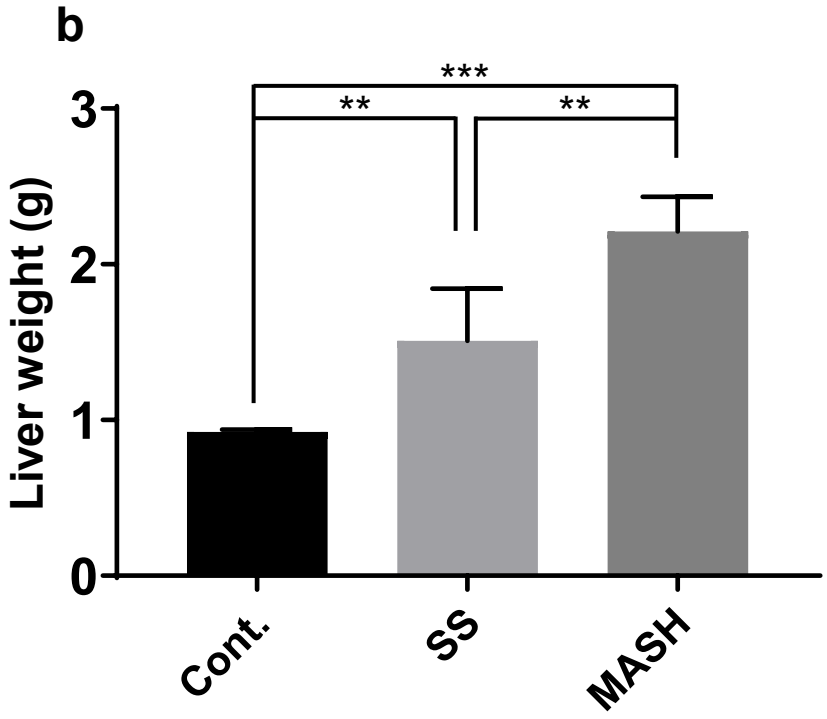
b
Liver weight (g)
3
2
1
0
***
**
**
Cont.
SS
MASH

Fig. 2

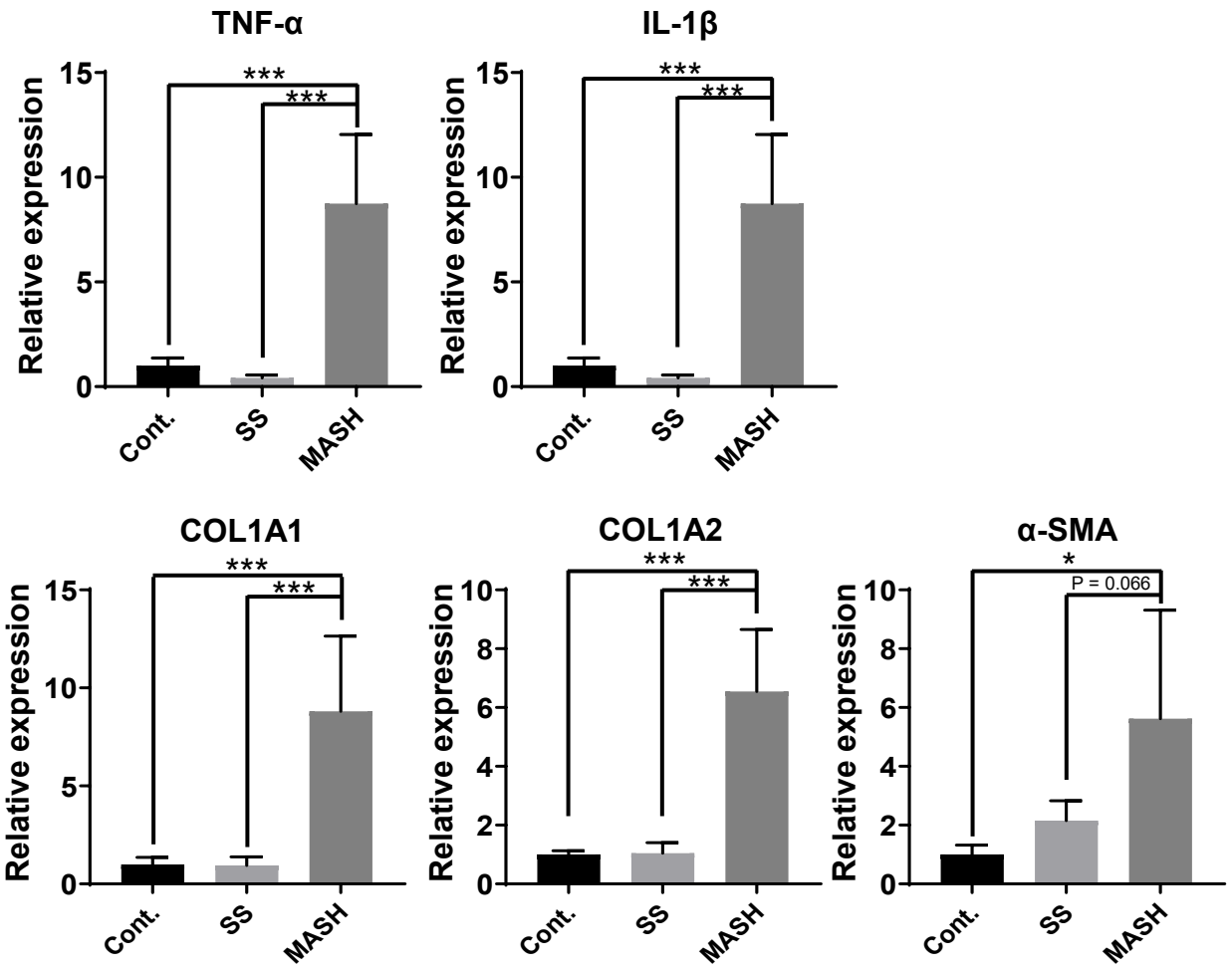
TNF-α
IL-1β
COL1A1
COL1A2
α-SMA
Relative expression
***
*
P = 0.066
Cont.
SS
MASH

Fig. 3

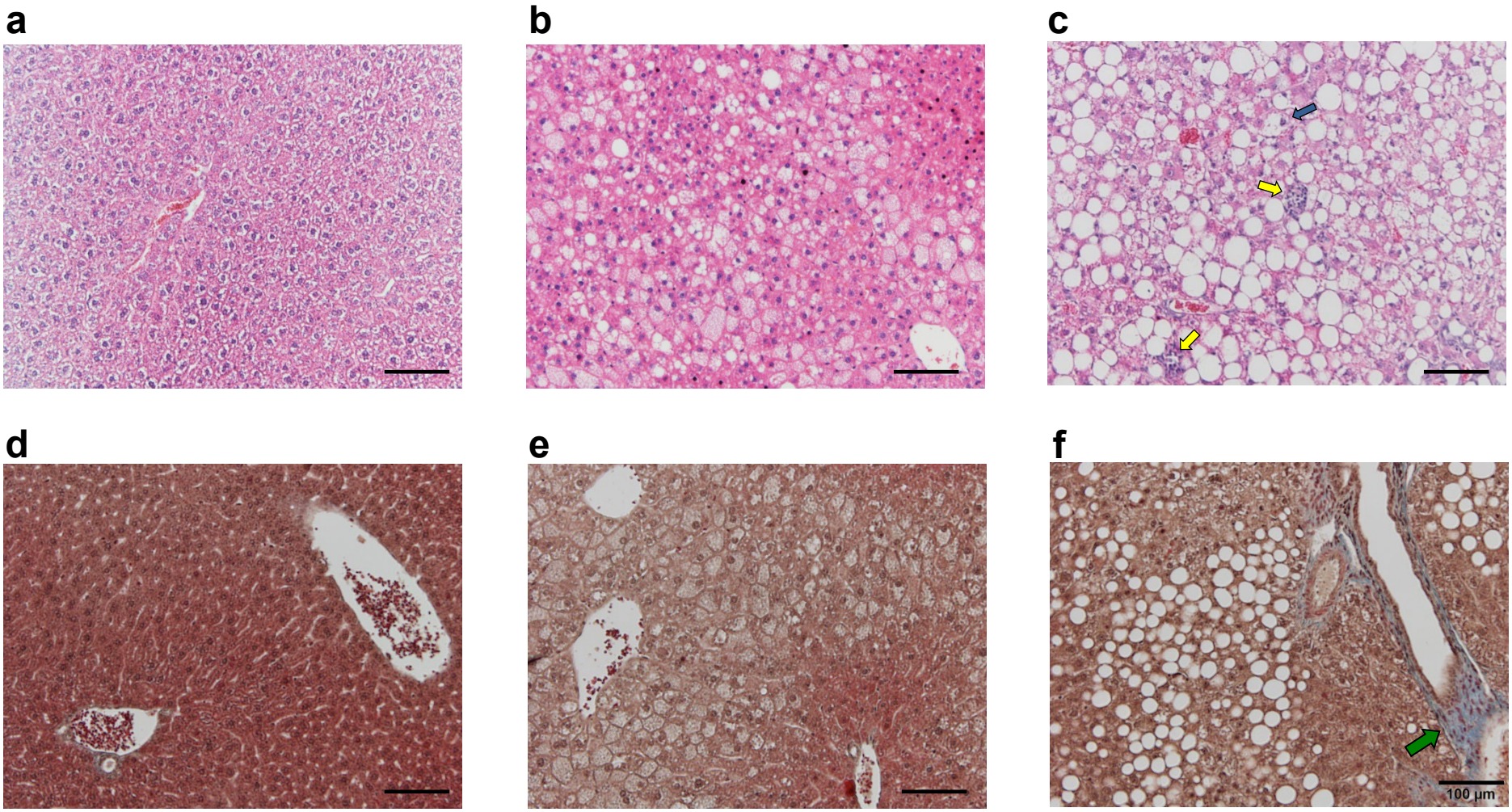

Fig. 4

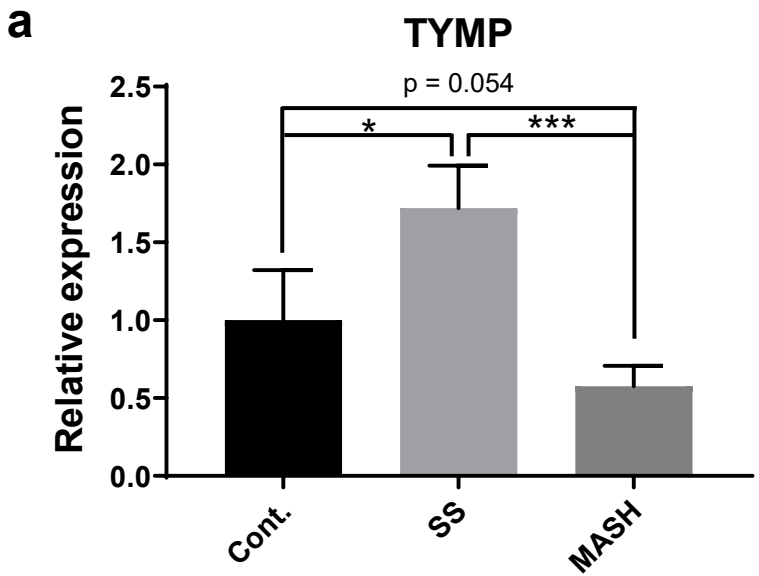
a
TYMP
p = 0.054
*
***
Relative expression
2.5
2.0
1.5
1.0
0.5
0.0
Cont.
SS
MASH

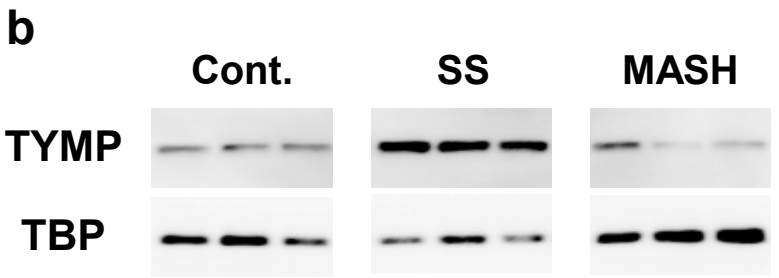
b
Cont.
SS
MASH
TYMP
TBP

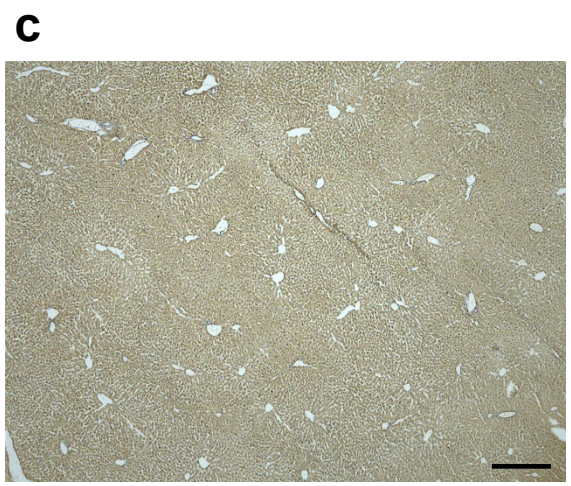
c

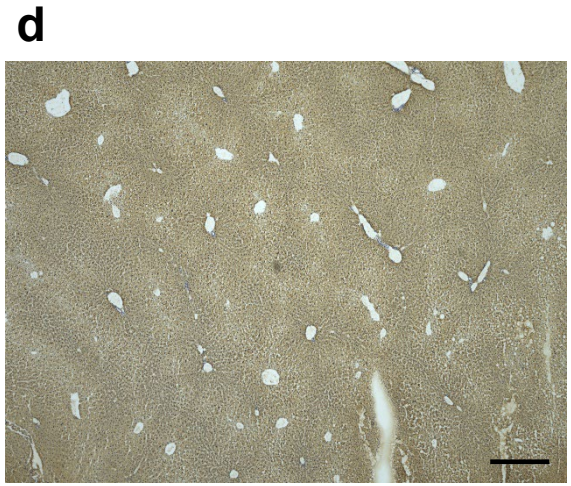
d

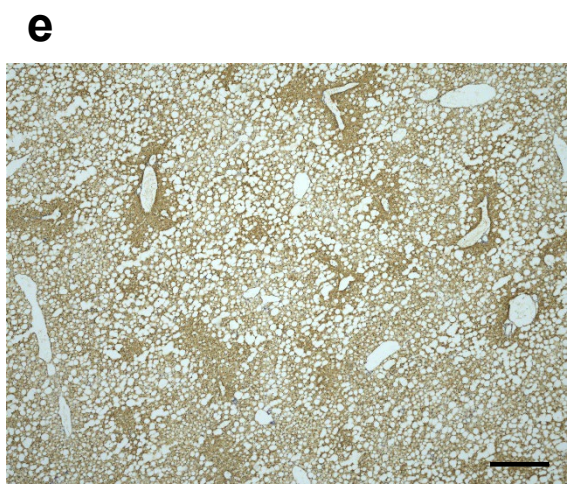
e

Fig. 5 (Revised in rev.2)

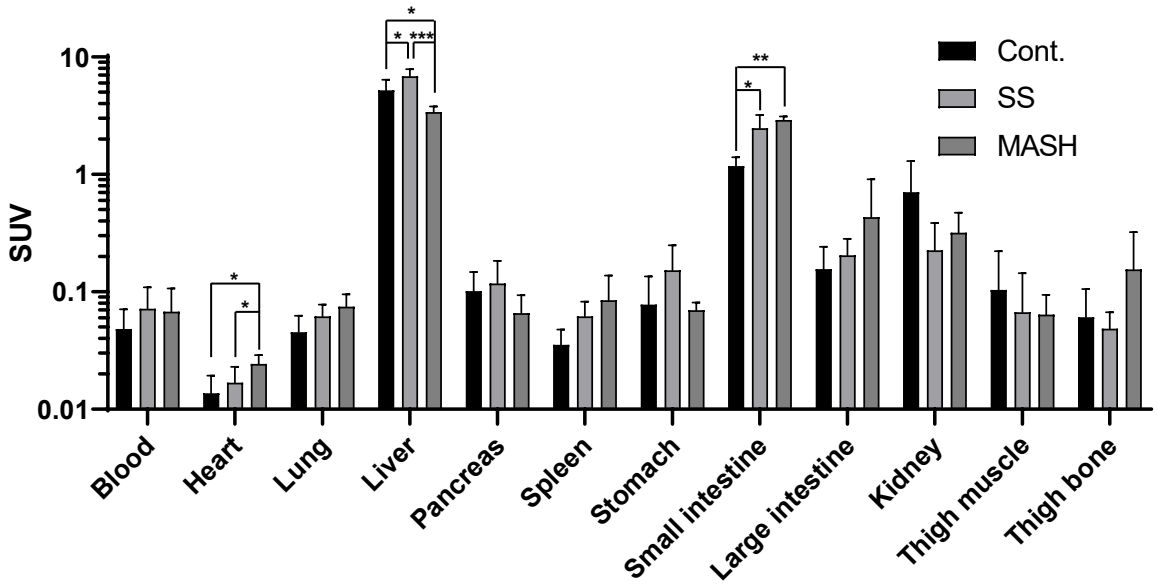

Fig. 6

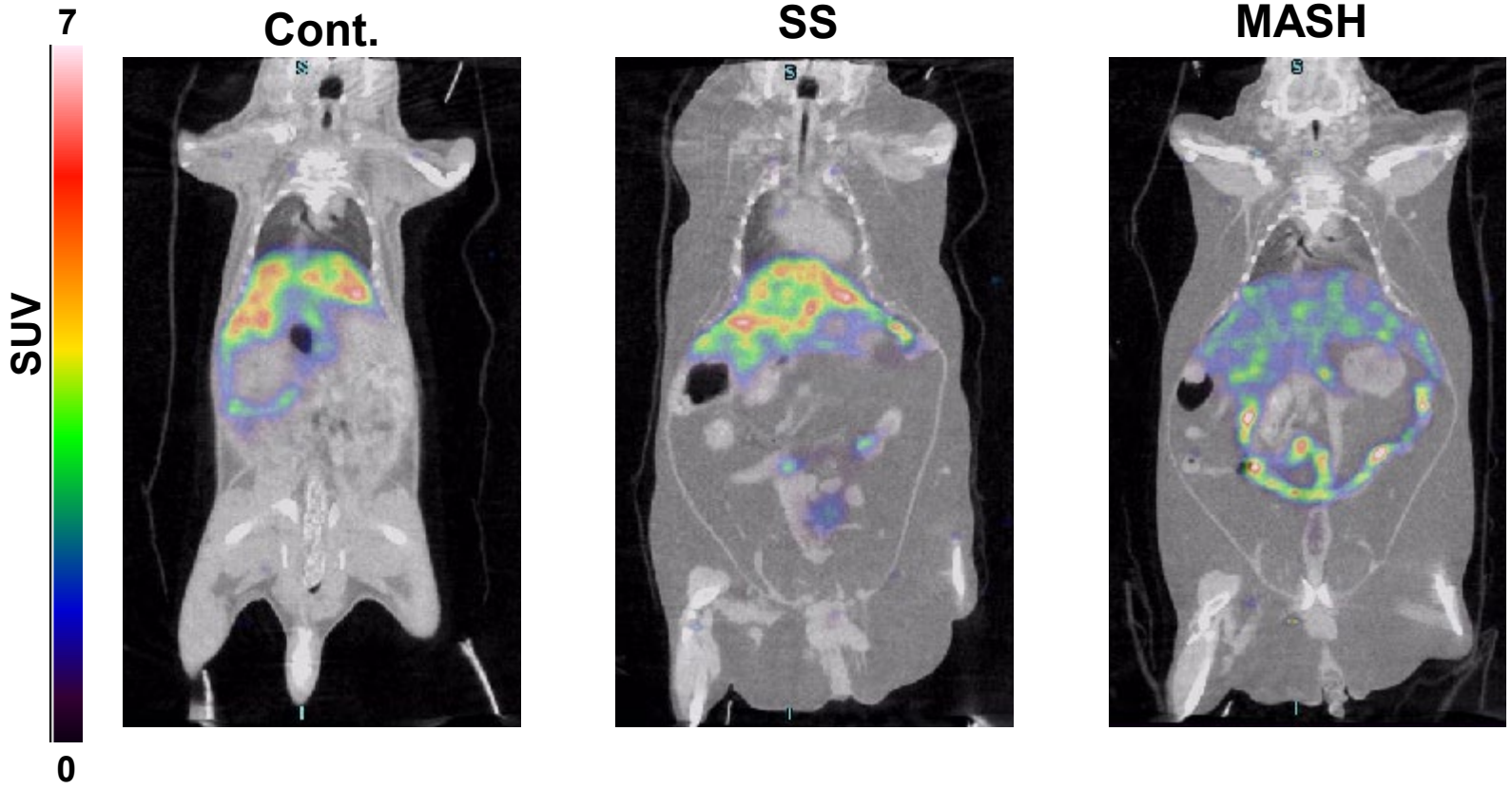

Electronic Supplementary Material

Title: Thymidine phosphorylase imaging probe for differential diagnosis of metabolic dysfunction-associated steatohepatitis

Journal: Molecular Imaging and Biology

Authors: Kei Higashikawa[1], Riho Uehara[2], Sawako Horiguchi[2], Yuki Shibata[1,3,4], Naoto Okubo[2], Yuki Mizuno[1,5], Hironobu Yasui[1,4], Shunsuke Ohnishi[2], Hiroshi Takeda[2], Yuji Kuge[1,5]

[1]Central Institute of Isotope Science, Hokkaido University, Sapporo 060-0815, Japan
[2]Faculty of Pharmaceutical Sciences, Hokkaido University, Sapporo 060-0812, Japan
[3]Graduate School of Biomedical Science and Engineering, Hokkaido University, Sapporo 060-0815, Japan
[4]Faculty of Veterinary Medicine, Hokkaido University, Sapporo 060-0818, Japan
[5]Global Center for Biomedical Science and Engineering, Faculty of Medicine, Hokkaido University, Sapporo 060-0815, Japan

*Corresponding Author:
Yuji Kuge, Ph.D.
Central Institute of Isotope Science, Hokkaido University
Kita 15, Nishi 7, Kita-ku, Sapporo 060-0815, Japan
Tel.: +81-11-706-6087
Fax: +81-11-706-7862
E-mail: kuge@ric.hokudai.ac.jp

Running title: TYMP imaging probe for MASH

Category: Original article

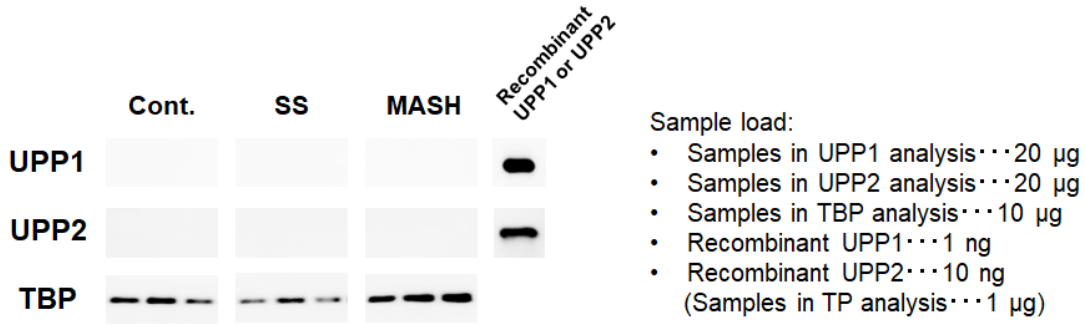

Fig. S1 UPP expression in the liver of the control, SS, and MASH mice. Hepatic protein expression levels of UPP1 and UPP2 were examined in the control, SS, and MASH mice (n = 3) by western blot analysis. Recombinant UPP1 (1 ng) and UPP2 (10 ng) are positive controls. TBP was used as a loading control.

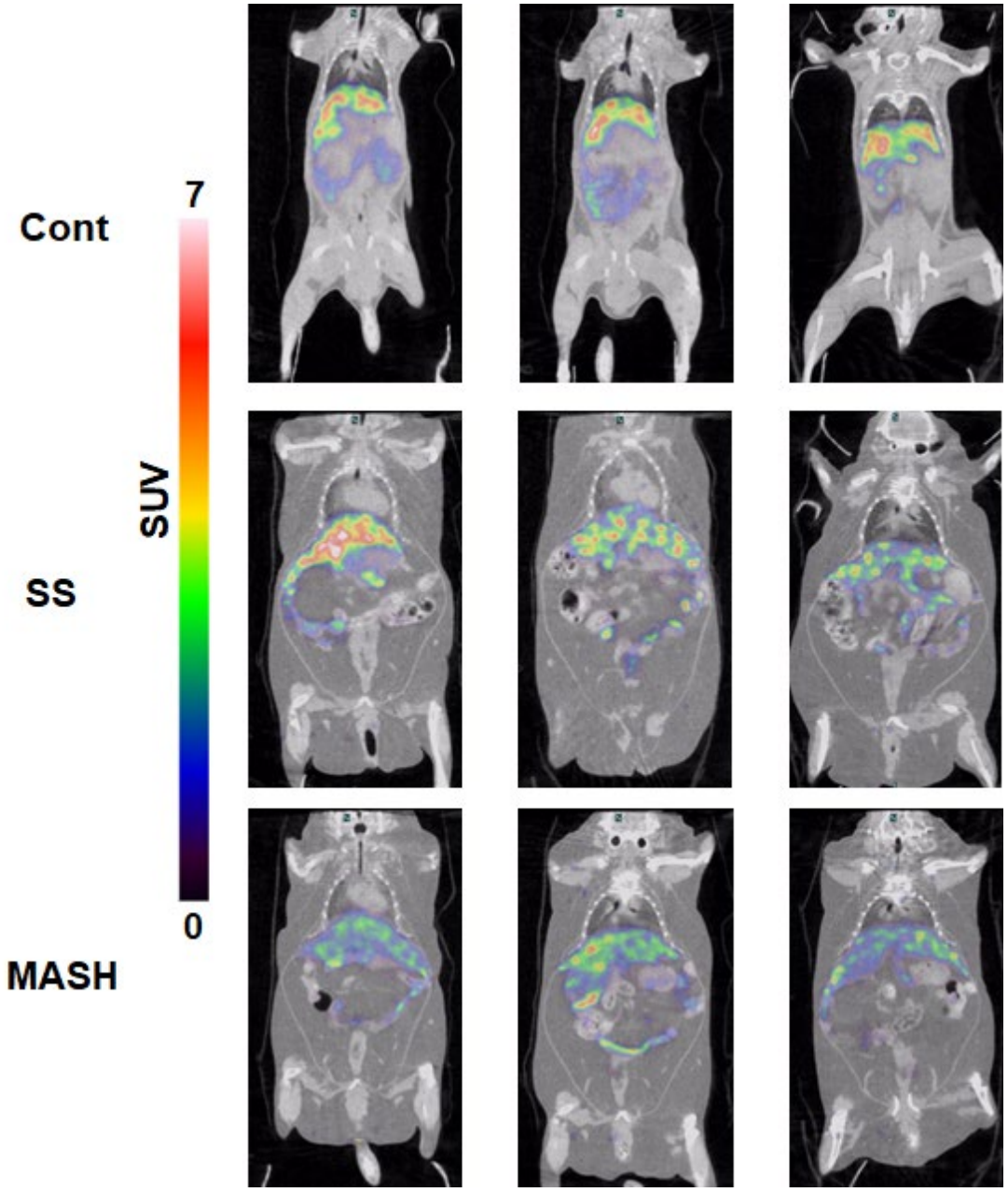

Fig. S2 Additional SPECT/CT images of control, SS, and MASH model mice after injection of [^{123}I]IIMU. All SPECT images (coronal slices) are displayed on the same SUV scale ranging from 0 to 7.

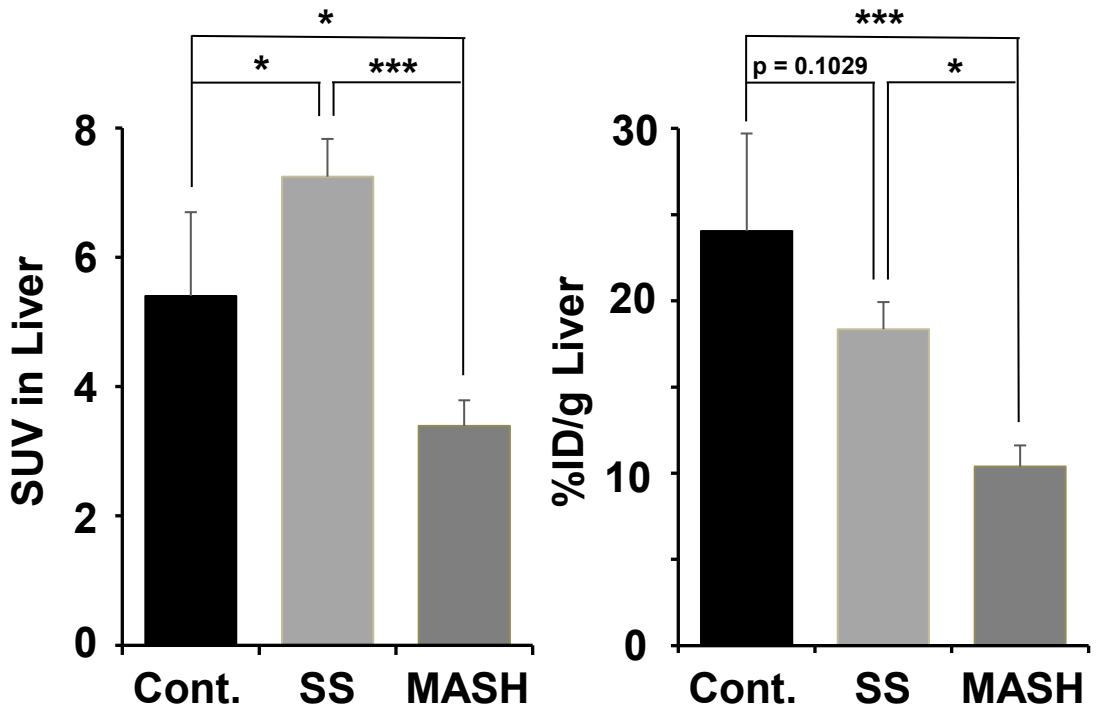

Fig. S3 Effects of the body weights on the hepatic [^{125}I]IIMU accumulation. (a) SUV, body weight-corrected values, and (b) %ID/g, non-corrected values, calculated using the same data as in Fig. 5. Data are expressed as means (bar: standard deviation). For statistical evaluation, one-way ANOVA followed by Tukey-Kramer's test was applied. The symbol * and *** denote $p < 0.05$ and $p < 0.001$, respectively.

Table S1

List of primer sequences for Real-time RT-PCR

Gene	Primer	Sequence (5' to 3')
TNF-α	Forward	ccccaaagggatgagaagtt
	Reverse	cacttggtggtttgctacga
IL-1β	Forward	ggtgtgtgacgttcccattag
	Reverse	tcgttgcttggttctccttg
COL1A1	Forward	ttcacctacagcacccttgtgg
	Reverse	tggagggagtttacacgaagcag
COL1A2	Forward	attgcgtacctggatgaggag
	Reverse	caggcgagatggcttatttg
α-SMA	Forward	ggatgcagaaggagatcacag
	Reverse	tagacagcgaagccaggatg
TBP	Forward	tgacccaccagcagttcag
	Reverse	caggagaacatggcagacaac